ResearchGate

See discussions, stats, and author profiles for this publication at: https://www.researchgate.net/publication/51855405

Magnetic Properties of Paddlewheels and Trinuclear Clusters with Exposed Metal Sites

ARTICLE *in* CHEMPHYSCHEM · DECEMBER 2011

Impact Factor: 3.42 · DOI: 10.1002/cphc.201100559 · Source: PubMed

CITATIONS
12

READS
63

4 AUTHORS, INCLUDING:

Konstantinos Dionisiou Vogiatzis
Karlsruhe Institute of Technology
8 PUBLICATIONS **123** CITATIONS
SEE PROFILE

Andreas Mavrandonakis
University of Minnesota Twin Cities
31 PUBLICATIONS **1,037** CITATIONS
SEE PROFILE

Available from: Andreas Mavrandonakis
Retrieved on: 26 January 2016

DOI: 10.1002/cphc.201100559

Magnetic Properties of Paddlewheels and Trinuclear Clusters with Exposed Metal Sites

Konstantinos D. Vogiatzis,[a] Wim Klopper,*[a, b] Andreas Mavrandonakis,[a] and Karin Fink[b]

Magnetic exchange-coupling constants of tri- and dinuclear transition-metal complexes (paddlewheels) have been computed using various ab initio methods. The di- and trinuclear complexes under study may serve as secondary building units in metal-organic frameworks (MOFs). Multi-reference methods such as the complete-active-space self-consistent-field method (CASSCF) as well as second-order perturbation theory (CASPT2) yield spin ladders from which the magnetic exchange-coupling constants are obtained. For the dicobalt paddlewheels, inclusion of spin–orbit coupling is crucial for obtaining a qualitatively correct description of the system. Density functional theory (DFT) was applied in the framework of the broken-symmetry approach using single- and double-hybrid functionals as well as generalized-gradient-approximation (GGA) functionals. The computed magnetic exchange-coupling constants are compared with experimental and other theoretical data, where available.

1. Introduction

The magnetic properties of two types of acetato-bridged transition metal compounds are examined. The first type of compounds are the tetra-μ-acetato-dimetal complexes $[M_2(OOCR)_4L_2]$ (Figure 1 a). Due to their characteristic shape, they are also known as paddlewheels. A variety of different complexes of this type have been synthesized and described, for example, by using different metal atoms. Compounds with various axial ligands such as $L = H_2O$ and NH_3 exist, as well as compounds without any axial ligands (undercoordinated metal centers). Furthermore, the R group in the bridge can be varied. The second type are trimetallic $[M_3O(OOCR)_6L_3]^{n+}$ complexes (for $R = -CH_3$, see Figure 1 b). Both types of compounds serve as secondary building units (SBU) in metal-organic frameworks (MOFs).[1] A typical example is $Cu_3(btc)_2$ (btc = benzene-1,3,5-tricarboxylate), also known as HKUST-1,[2] in which Cu paddlewheels are coordinated with benzene-1,3,5-tricarboxylate forming a zeolite-type porous material. In particular, $Cu_3(btc)_2$ has the important feature in that the axial water ligands can be removed from the metal sites by heating, and the structure does not collapse upon removal of the solvent and retains its periodicity and porosity. Recently, the applicability of such undercoordinated metal sites of porous materials was demonstrated.[1,3] The open metal sites showed Lewis acid catalytic properties.[3,4] Hydrogen storage characteristics were also reported to be significanctly enhanced with respect to other MOFs with fully coordinated metal sites. The enhancement is attributed to the stronger interaction of dihydrogen with the open metal centers by means of a Kubas-type interaction.[5]

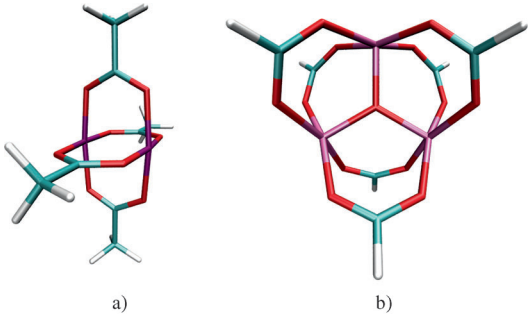

Figure 1. a) Tetra-μ-acetato-dimetal and b) $[M_3O(OOCCH_3)_6]^{n+}$ structures. Color code: M: purple, O: red, C: blue, H: white.

Herein, we concentrate on the magnetic properties of the SBUs. The coupling of the local spins of paramagnetic centers in molecules and solids gives rise to molecular magnetic properties similar to ferromagnetism and antiferromagnetism. Molecule-based magnetic materials may become of technical interest because they may be used to store and process information at the molecular level.[6]

The complexes that are examined herein are the diaqua-tetra-μ-formato-dinuclear family of molecules, which constitute the core of the paddlewheel-type SBUs. Copper, manganese

[a] K. D. Vogiatzis, Prof. W. Klopper, Dr. A. Mavrandonakis[+]
Center for Functional Nanostructures (CFN) and
Institute of Physical Chemistry
Karlsruhe Institute of Technology
KIT Campus South, P.O. Box 6980, 76049 Karlsruhe (Germany)
Fax: (+49) 721 60847225
E-mail: klopper@kit.edu

[b] Prof. W. Klopper, Dr. K. Fink
Institute of Nanotechnology (INT)
Karlsruhe Institute of Technology
KIT Campus North, P.O. Box 3640, 76021 Karlsruhe (Germany)

[+] Current address:
School of Engineering and Science, Theoretical Physics
Jacobs University Bremen
Campus Ring 1, 28759 Bremen (Germany)

 © 2011 Wiley-VCH Verlag GmbH & Co. KGaA, Weinheim

and cobalt were chosen as metal centers of the homo-dinuclear complexes. Little is known of the magnetic properties of these compounds. Few studies for the copper(II) formate have been reported into the literature[7] while the anhydrous cobalt(II) and manganese(II) paddlewheels have not been studied previously.

We shall first and foremost investigate the magnetic properties of the copper(II) paddlewheel. There is a vast literature for the diaqua-tetra-μ-acetato-dicopper red complex, both experimentally and computationally (see ref. [8] and references therein). Thus, the starting point of our study is this compound, whose results are used for calibrating our methods. On the dicopper(II) compound, each metal cation has only one unpaired electron with the coupling between the two Cu^{II} centers being antiferromagnetic. In other words, the spin ground state is a singlet $S=0$. The strong competition between direct exchange, superexchange and higher-order mechanisms makes it an interesting system for theoretical investigations.[8] Almost every new proposed method or model that describes magnetic coupling has been tested on this compound.

We extend our study to trimetallic anhydrous formates, which can also form MOFs with open-metal sites after successful removal of the axial ligands. Experimentally, the trinuclear iron(II), chromium(III) and vanadium(III) clusters have been the target of magnetic susceptibility studies but their hydrated analogues have not.[9] Of particular interest is the chromium analogue, since it acts as a catalyst in cyanosilylation.[10] Therefore, the hydrated and anhydrous chromium(III) formates are included in our study.

2. Theoretical Aspects

The magnetic properties of polynuclear transition metal compounds originate from the coupling of the electronic configurations at the different metal centers. The unpaired *d* electrons at each center *i* are coupled to a local spin S_i. These local spins can be coupled to different total spin states which differ only slightly in energy. The number of low-lying electronic states and their energies can often be described by phenomenological model spin Hamiltonians.

We use a Heisenberg–Dirac–van Vleck (HDV) model spin Hamiltonian for the description of the magnetic properties. For the dimetallic systems, this Hamiltonian is given by Equation (1):

$$H^{\mathrm{HDV}} = -2J\left(\vec{S}_1 \cdot \vec{S}_2\right) \tag{1}$$

where J is the magnetic exchange coupling constant. For two local spins S_1 and S_2, the total spin can have the values $S = S_1 + S_2, S_1 + S_2 - 1, \ldots, |S_1 - S_2|$. The energy levels correspond to a simple Landé pattern and are given by Equation (2):

$$E(S) = -J[S(S+1) - S_1(S_1+1) - S_2(S_2+1)] \tag{2}$$

For the trimetallic systems, the Hamiltonian associated with the weak antiferromagnetic coupling is the sum of the pair interactions [Eq. (3)]:

$$H = -2J_{12}\left(\vec{S}_1 \cdot \vec{S}_2\right) - 2J_{23}\left(\vec{S}_2 \cdot \vec{S}_3\right) - 2J_{31}\left(\vec{S}_3 \cdot \vec{S}_1\right) \tag{3}$$

With threefold symmetry, this reduces to Equation (4):

$$H = -2J\left(\vec{S}_1 \cdot \vec{S}_2 + \vec{S}_2 \cdot \vec{S}_3 + \vec{S}_3 \cdot \vec{S}_1\right) \tag{4}$$

and the corresponding energy levels are given as Equation (5):

$$E(S) = -J[S(S+1) - 3S_1(S_1+1)] \tag{5}$$

where S_1 is the spin on each of the metal centers and S is the total spin of the complex.[9] The values of S and occurring degeneracies in the trinuclear compounds are discussed in the last section. For negative values of J the compounds are antiferromagnetic, for positive J they are ferromagnetic.

We obtained the magnetic exchange coupling constants J from two completely different quantum chemical approaches. On the one hand, we performed calculations on all different spin states of the bi- and trinuclear compounds. In these calculations, the treatment of the systems with multi-reference methods is mandatory and dynamical electron correlation has to be included.[11,12] Multi-reference calculations were performed at the complete-active-space self-consistent-field (CASSCF) and second-order perturbation theory (CASPT2) levels. In case of the dicobalt formates, each metal center possesses spatially almost degenerate states. All of these states have to be included in the calculations and the spin–orbit interaction of these states was obtained by diagonalizing the Hamiltonian [Eq. (6)]:

$$\langle \mu | H_0 + H_{\mathrm{SOC}} | \nu \rangle \tag{6}$$

where μ and ν are CASSCF wavefunctions of low-lying states. H_0 denotes the nonrelativistic Hamiltonian and H_{SOC} refers to the one- and two-electron spin–orbit interaction.

On the other hand, the broken-symmetry method with various generalized gradient approximations (GGA) and hybrid density functionals was applied. Density functional theory (DFT) succesfully describes high-spin (HS) states but normally fails for the low-spin (LS) states. An alternative description for the LS states is based on the broken spin and space symmetry single-determinant wavefunction as suggested by Noodleman more than twenty years ago.[13,14] This broken-symmetry (BS) state is not a pure spin state, but a weighted average of these. Nevertheless, the energy difference between the HS and BS states can provide an estimate of the magnetic exchange coupling constant. In terms of the BS approach—justified by Moreira and Illas[8]—the energy eigenvalue spectrum of the HDV Hamiltonian for the dimetallic systems can be approximated by the coupling constants obtained from the Ising Hamiltonian [Eq. (7)]:

 © 2011 Wiley-VCH Verlag GmbH & Co. KGaA, Weinheim

$$H^{\text{Ising}} = -2JS_{z_1}S_{z_2} \quad (7)$$

Depending on spin projection, different equations exist for mapping the BS energies onto the states of the HDV Hamiltonian. Herein, we use the equation originally proposed by Noodleman, Equation (8):

$$J^{\text{BS}} = -\frac{E_{\text{HS}} - E_{\text{BS}}}{4S_1S_2} \quad (8)$$

Yamaguchi[15] introduced an expression that includes the total spin angular momentum expectation values of the HS and BS Kohn–Sham determinants [Eq. (9)]:

$$J^{\text{BS}} = -\frac{E_{\text{HS}} - E_{\text{BS}}}{\langle S^2\rangle_{\text{HS}} - \langle S^2\rangle_{\text{BS}}} \quad (9)$$

For the bimetallic systems, the same results are obtained with both approaches.

Without symmetry restrictions, there are three BS states for the trimetallic systems. The coupling constants can then be obtained in the same manner as in ref. [16] from the HS and the BS states by mapping the eigenvalues of the Ising operator onto the Heisenberg Hamiltonian.[8]

Besides GGA and hybrid functionals, the double-hybrid density-functional approach (DHDF) is also examined. The DHDF approach consists of mixing the standard GGA functional for exchange by Becke (B88) with the standard GGA functional for correlation by Lee, Yang and Parr (LYP), with Hartree–Fock exchange, and with a second-order perturbation theory part.[17] The total exchange–correlation energy is calculated by Equation (9):

$$\begin{aligned} E_{\text{XC}}^{\text{DHDF}} =& (1-\alpha_x)E_{\text{X}}^{\text{GGA}} + \alpha_x E_{\text{X}}^{\text{HF}} \\ &+ (1-\alpha_c)E_{\text{C}}^{\text{GGA}} + \alpha_c E_{\text{C}}^{\text{KS-PT2}} \end{aligned} \quad (10)$$

where $E_{\text{X}}^{\text{GGA}}$ is the energy of a conventional exchange functional and $E_{\text{C}}^{\text{GGA}}$ is the energy of a correlation functional. E_{X}^{HF} is the Hartree–Fock exchange of the occupied Kohn–Sham (KS) spin orbitals and $E_{\text{C}}^{\text{KS-PT2}}$ is a Møller–Plesset-like perturbation correction term based on KS spin orbitals Eq. (11):

$$E_{\text{C}}^{\text{KS-PT2}} = \frac{1}{4}\sum_{ia}\sum_{jb}\frac{[(ia|jb) - (ib|ja)]^2}{e_i + e_j - e_a - e_b} \quad (11)$$

The method is self-consistent only with respect to the first three terms in Equation (10). Based on the self-consistent orbitals, $E_{\text{C}}^{\text{KS-PT2}}$ is evaluated afterwards and added to the total energy. The exchange–correlation energy, as proposed by Grimme (B2-PLYP),[18] is composed of B88 for exchange and LYP for correlation, with the values $a_x = 0.53$ and $a_c = 0.27$ for the two parameters. It has been shown that this approach yields better results than several popular functionals (BMK, B3LYP, TPSSh). In specific cases, it outperforms the MP2 method, where spin contamination of the Hartree–Fock reference is present, for example in radicals.

Recently, it has been shown (mostly for simple model systems and organic compounds) that the DHDF approach can succesfully be applied in BS calculations.[19] Only one model system with two metal atoms was included herein and thus, we investigate whether the DHDF appraoch can be applied to other metallic systems. Indeed, the coupling constants obtained from B2-PLYP theory agree better with experimental results than those obtained from other functionals.

Computational Details

Geometry optimizations were performed for the high-spin states. The structures were optimized at the unrestricted MP2/def2-TZVP[20] (UMP2) level of theory with the ricc2 program[21] of the TURBOMOLE[22,23] program package under symmetry restrictions D_{2h} and D_{3h} for the dimetallic and trimetallic systems, respectively. Vibrational frequencies were computed by numerical differentiation of the gradient. For $[Cu_2(OOCCH_3)_4(H_2O)_2]$ the obtained structural parameters were compared to available X-ray data. The Cu–O bond length differed by less than 0.01 Å, the Cu–Cu distance by about 0.01 Å and the Cu–O–C angle by 2.1° from the experimental values.[24–26] We assume that the structures of the other compounds have the same accuracy, and in the next sections, comparisons will be given with crystallographic data of similar structures, where available.

Based on these structures, CASSCF/CASPT2 calculations were performed with the MOLPRO[27] program package. Starting orbitals were obtained from a restricted open-shell Hartree–Fock (ROHF) calculation for the high-spin state for each molecule. For most systems, the active space for the subsequent calculations was equivalent to the singly occupied orbitals of the high-spin state, as computed at the ROHF level. In case of the dicobalt formate and trichromium compounds, a state-averaged (SA) CASSCF calculation was performed after the ROHF calulation for all high-spin states close in energy. This procedure provided a complete set of *d* orbitals of similar accuracy as active space. With the CASSCF optimized orbitals we performed CASPT2 calculations. In the multi-reference calculations, the cc-pVTZ basis set for the metal atoms and the cc-pVDZ basis for all other atoms were used. All basis sets had been obtained from the EMSL basis-set exchange.[28]

The coupling constants from the BS approach were calculated with the TURBOMOLE program package. In addition to the double-hybrid B2-PLYP[18] functional, the BP86,[29] PBE[30] and TPSS[31] GGA functionals as well as the TPSSh[32] and B3LYP[33,34] hybrid functionals were tested. For all DFT calculations, the def2-TZVP[20,35] basis set was used.

3. Results and Discussion

3.1. Dinuclear Copper(II) Paddlewheel

Diaqua-tetra-μ-acetato-dicopper(II) molecule (dicopper acetate) was the starting point of our study, motivated by the existence of experimental data for comparison. It is an antiferromagnetic molecule with an experimental value for the magnetic coupling constant of $2J = -286\ \text{cm}^{-1}$, obtained from the temperature dependence of the magnetic susceptibility .[24] From a more recent inelastic neutron scattering (INS) study, a value of

 © 2011 Wiley-VCH Verlag GmbH & Co. KGaA, Weinheim

$2J = -298\ cm^{-1}$[36] was obtained. Note that the definition of J is not unique. All J values given herein correspond to the HDV Hamiltonian given in Equation (1).

Magnetic studies on the anhydrous paddlewheel are sparse, but an experimental J value of $-151\ cm^{-1}$[24] was obtained from a magnetic measurement of the anhydrous molecule between 90 °C and 400 °C. In the same study, the coupling constant for the hydrated compound was $J = -143\ cm^{-1}$, only $6\ cm^{-1}$ less than the more accurate INS study.[36]

Apart from the hydrated and anhydrous dicopper acetate, a second structure was also studied in order to have a more compact and computationally affordable model. In this model, the acetates were substituted by formate ligands. The geometry of the anhydrous formate was obtained from UMP2 theory for the triplet state. The optimized geometry shows an intermetallic distance of 2.53 Å, which is in agreement with experimental data for the dehydrated paddlewheel.[26] In the experimental study, the geometry was analyzed by extended X-ray absorption fine structure spectroscopy (EXAFS) and the Cu–Cu distance was found at 2.50 Å.

A free Cu^{II} ion has one unpaired electron due to its d^9 electronic configuration. This electron occupies the $d_{x^2-y^2}$ orbital under the specific ligand field of the paddlewheel structure, which is of square planar symmetry for each of the copper atoms. The active space for the CASSCF/CASPT2 calculations includes two molecular (magnetic) orbitals which are composed of the symmetric and antisymmetric combinations of the two singly occupied $d_{x^2-y^2}$ atomic orbitals. These molecular orbitals include also small contributions from the p orbitals of the oxygens. The two electrons in the two molecular orbitals—a (2,2) active space for short—yield two configurations for the singlet state. These configurations have almost the same weight [0.49 and 0.51 squared configuration-interaction (CI) coefficients], and the ground state is a singlet. The electronic structure is the same for the hydrated and anhydrous paddlewheels.

CASSCF(2,2) calculations for the dicopper acetate hydrate yielded a magnetic coupling constant of $-11.0\ cm^{-1}$. The addition of dynamical correlation alters this value to $J = -55.3\ cm^{-1}$ at the CASPT2(2,2) level. Both values are far from the experimental value ($-149\ cm^{-1}$) but are in agreement with other theoretical studies on the same compound, in which CASSCF theory predicted a J value between -9.5 and $-12.1\ cm^{-1}$ and CASPT2 a value of $-56.5\ cm^{-1}$.[8,37,38]

CASPT2 introduces second-order effects resulting mainly from the superexchange mechanism and the double-spin polarization. There are two main reasons that CASPT2 lacks part of the superexchange coupling, when compared with experimental data. First, and most important, this is due to the lack of convergency of the perturbation series.[11] Second, a minimal complete active space with two electrons in two orbitals was used. More sophisticated but computationally also more demanding methods such as the difference-dedicated configuration-interaction (DDCI)[39,40] method recover more correlation energy. DDCI3 applied to the Cu dimer acetate complex predicts $J = -113\ cm^{-1}$.[8] From a recent article by Neese et al.,[38] a highly accurate coupling constant was reported ($-137\ cm^{-1}$) from the DDCI3 level of theory. From the same study, the DDCI2 value was $-33.8\ cm^{-1}$. DDCI3 does not only include one hole/one particle single excitations and two holes/two particles double excitations which are present in DDCI2, but also two holes/one particle and one hole/two particles excitations, which play an important role for the kinetic exchange contribution.

For the anhydrous dicopper acetate, slightly more negative values were obtained with the same methods. Similarly to the hydrated compound, an active space of two electrons in two orbitals was used. CASSCF(2,2) predicts $J = -13.1\ cm^{-1}$ and CASPT2(2,2) predicts $J = -65.9\ cm^{-1}$. These results are consistent with the respective differences between the experimental and theoretical values for the hydrated paddlewheel (Table 1).

Table 1. Multi-reference and BS results for the hydrated and anhydrous dicopper paddlewheels [cm^{-1}].

Method	Dicopper Acetate		Dicopper Formate	
	Hydrated	Anhydrous	Hydrated	Anhydrous
CASSCF	−11.0	−13.1	−14.3	−16.8
CASPT2	−55.3	−65.9	−72.8	−91.3
BP86	–	–	−1477	−1371
PBE	–	–	−1496	−1387
TPSS	–	–	−1133	−1057
TPSSh	–	–	−618	−616
B3LYP	−229	−275	−438	−467
B2-PLYP	−145	−166	−213	−260
Magnetic Susceptibility	−143[24]	−151[24]	−275[7]	–
INS	−149[36]	–	–	–

Absence of the axial water molecule results in a 6% more negative experimental magnetic coupling constant. This ratio is significantly larger for the multi-reference methods (about 18%) and for the BS approach with the B3LYP functional (20%). It is 14% for the B2-PLYP approach.

The same trends were observed when applying the multi-reference methods to the dicopper formates (Figure 2). Differences between CASSCF and CASPT2 were similar to those of the acetate paddlewheels, with CASPT2 giving almost five times stronger coupling constants than CASSCF. For example, for the hydrated compound, the multi-reference methods pre-

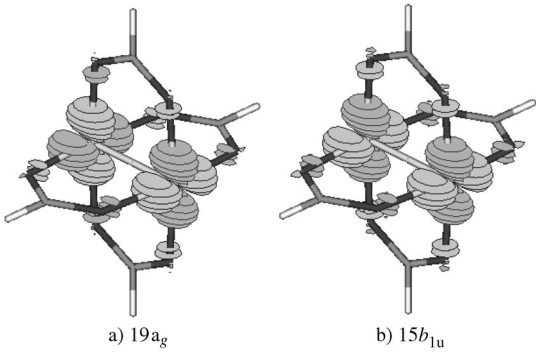

Figure 2. Magnetic orbitals forming the (2,2) active space in the anhydrous dicopper formate.

 © 2011 Wiley-VCH Verlag GmbH & Co. KGaA, Weinheim

dict $-14.3\ cm^{-1}$ (CASSCF) and $-72.8\ cm^{-1}$ (CASPT2). In this case there is no agreement with the experimental value of $-275\ cm^{-1}$, but unfortunately, neither sufficient experimental details nor the axial ligands are given in ref. [7]. According to our calculations, we conclude that the magnetic coupling constant should be lower for the dicopper formate hydrate than for the acetate. Experimental results are not available for the anhydrous dicopper formate. With respect to the latter, we found more negative J values than for the aforementioned compounds, with the magnetic coupling constant computed at $J=-16.8\ cm^{-1}$ from CASSCF(2,2) and $J=-91.3\ cm^{-1}$ from CASPT2(2,2) theory.

The effect of correlating the core orbitals was studied at the CASPT2 level. For example, for the anhydrous dicopper acetate, the frozen-core (FC) approximation yields $J=-87.5\ cm^{-1}$ when 46 orbitals are correlated. The orbitals kept frozen are the 1s, 2s, 2p, 3s and 3p orbitals of the two coppers and the 1s orbitals of the carbons and oxygens. By correlating all the 76 orbitals (74 doubly and two singly occupied orbitals), the CASPT2 approach yields $J=-91.3\ cm^{-1}$. The contribution from dynamical correlation to the magnetic coupling constant of course depends on the orbitals that are correlated, but the FC approximation can be used without introducing significant errors.

The dependence of the exchange coupling constant on the basis set was also examined. Different combinations of basis sets were tested on the anhydrous dicopper formate. When either increasing or decreasing the basis set of Cu^{2+} (Table 2), or increasing the basis sets of all other atoms (Table 3), the

Table 2. Cu basis-set dependence of the anhydrous dicopper formate (J in cm^{-1}). The cc-pVDZ basis set is used for the remaining atoms.

	CASSCF	CASPT2
cc-pVDZ	−17.3	−91.9
cc-pVTZ	−16.8	−91.3
cc-pVQZ	−16.6	−91.2

Table 3. O, C, and H basis-set dependence of the anhydrous dicopper formate (J in cm^{-1}). The cc-pVTZ basis set is used for Cu.

	CASSCF	CASPT2
cc-pVDZ	−16.8	−91.3
cc-pVTZ	−16.6	−90.1
cc-pVQZ	−16.3	−88.4

effect on the J value is negligible. For example, by increasing the basis set of the oxygens, carbons and hydrogens, a decrease of about $3\ cm^{-1}$ was observed at the CASPT2 level, while the computation time with the cc-pVQZ basis set was almost 100 times longer than with the cc-pVDZ basis set. The choice of a triple-zeta basis set for the metal atoms and double-zeta basis sets for the other atoms seemed reasonable. These basis sets will be used for the compounds studied below.

To obtain further insight into the coupling mechanism, calculations were also conducted for a model system in which the bridging formate molecules were substituted by water molecules and hydroxide anions. At each Cu^{2+} ion, two OH^- and two H_2O ligands were added to obtain a neutral cluster (Figure 3). The positions of the hydrogens of the model system

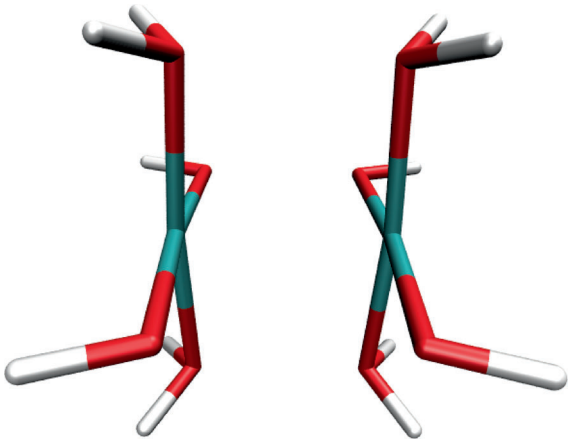

Figure 3. Model system for the copper formate hydrate, in which the bridging formate molecules are substituted by water molecules and hydroxide anions.

were optimized while the other atoms were kept fixed as in the original geometry. The CASSCF result was only $J=-1.16\ cm^{-1}$, whereas at the CASPT2 level $J=-13.2\ cm^{-1}$ was obtained. This indicates that the coupling is increased by superexchange.

The extent of the superexchange mechanism was different for the compounds with acetate and formate ligands, respectively. However, for both compounds, the Cu–O bond length (1.94 Å) and the O–C–O angle (125.5 °C and 127.5 °C) are almost identical. The magnetic orbitals of the CASSCF(2,2) calculation are also identical for both compounds (as in Figure 2). Thus, the main contribution should come from the different electron density of the carbons, which is dependent on the presence of methyl groups.

DFT calculations with the BS approach were also performed and results are presented in Table 1 for all copper paddlewheels. GGA functionals significantly overestimate the magnitude of the exchange coupling constants. For the hydrated dicopper formate, they predict values that are almost four to five times more negative than the available experimental values. Hybrid functionals are in better agreement but still far from experiment. B3LYP, for example, predicts a J value almost twice the experimental one. Results from the double-hybrid B2-PLYP approach are in better agreement with the experimental values than the GGA results. For the anhydrous acetate paddlewheel, the B2-PLYP result was $15\ cm^{-1}$ more negative than the experimental value, while for the hydrated one the difference was only $4\ cm^{-1}$. From a general comparison between BS and experimental values for all of the copper compounds, we conclude that B2-PLYP is superior to any other functional.

 © 2011 Wiley-VCH Verlag GmbH & Co. KGaA, Weinheim

Analogous to CASPT2, the exchange coupling is only slightly changed by not correlating the core orbitals. For example, using the frozen-core approximation for both the high-spin- and broken-symmetry states, the magnetic coupling constant for the dicopper acetate hydrate was estimated at $J=-137\ cm^{-1}$. On the other hand, with a full correlation treatment, the result is $8\ cm^{-1}$ more negative ($J=-145\ cm^{-1}$). This result differs only $4\ cm^{-1}$ from the experimental value. All B2-PLYP results in Table 1 were obtained without the frozen-core approximation.

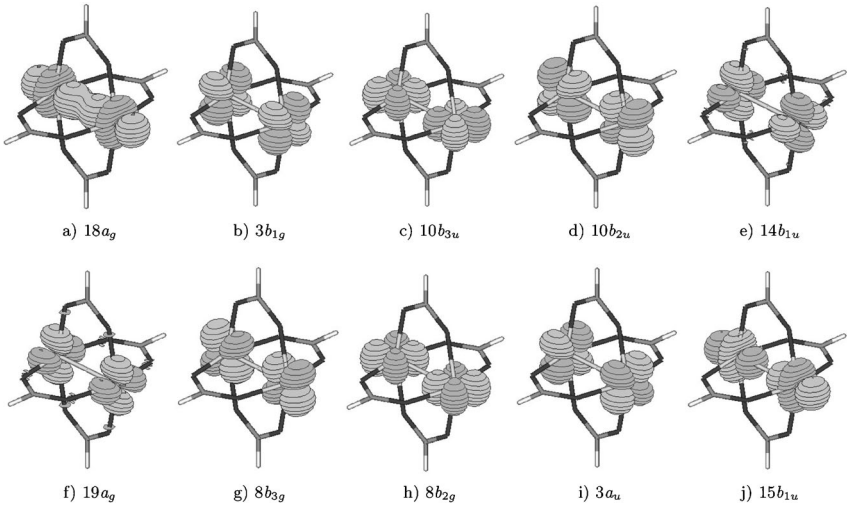

Figure 4. Magnetic orbitals forming the (10,10) active space of the manganese paddlewheel.

The performance of two recent families of exchange-correlation functionals, the range-separated hybrid functionals and the M06 functionals, for describing the electronic structure and the magnetic coupling constant, has been tested on a set of systems with two unpaired electrons.[41,42] In these studies, the hydrated dicopper acetate system was also included. In particular, the value obtained from the range-separated LC-ωPBE functional[43] ($J=-137\ cm^{-1}$) is in perfect agreement with the experimental data and our B2-PLYP value.

Table 4. Computed J values for the anhydrous dimanganese formate [cm^{-1}].

Method	Level Shift	J
CASSCF		−6.70
CASPT2[a]	0.1	−18.8
	0.2	−17.6
	0.3	−17.0
B3LYP		−31.7/−26.5[a]
B2-PLYP		−22.4/−18.6[b]

[a] With frozen-core approximation. [b] From unprojected expression, Equation (12).

3.2. Dinuclear Manganese(II) Paddlewheel

In contrast to the dicopper molecules described in Section 3.1, only a few manganese paddlewheel structures have been reported in the literature. The first metal-organic framework (MOF) with a manganese paddlewheel core was published in 2008 by Fu et al.[44] In the work of these authors, the Mn–Mn distance is 3.06 Å. The same Mn–Mn distance was found in our UMP2 optimization of the anhydrous manganese formate.

Recently, a systematic study of the magnetochemistry of dinuclear manganese complexes was published,[45] including also dimanganese compounds bridged with four acetate molecules. In that study, saturated Mn^{III} and Mn^{IV} centers were examined, but not Mn^{II} ions with open sites in their ligand spheres.

A free Mn^{II} ion has a d^5 electronic configuration with a ^6S ground state, which is a very stable configuration (half-filled shell). In the dimetallic structure, ten electrons occupy ten d orbitals and a (10,10) active space was chosen for the multi-reference treatment of the anhydrous compound (Figure 4). Both CASSCF and CASPT2 approaches predict an antiferromagnetic behavior, reproducing perfectly a spin-ladder from the singlet to the highest spin state of 10 unpaired electrons. The singlet state was constructed from 2528 configurations, with 133 having a CI coefficient between 0.05 and 0.084. The magnetic coupling constant was computed from Equation (2). The obtained values and the energy differences are presented in Table 4. In comparison with the hydrated or anhydrous Cu^{II} paddlewheels, the absolute values of the exchange coupling constant are significantly smaller.

CASPT2 calculations cannot be converged when intruder states occur with zeroth-order energy close or below the reference energy. This may happen when weakly occupied orbitals have energies close to those of external orbitals or strongly occupied orbitals close to those of inactive orbitals. The energy denominators of excitations into or out of the active orbitals can then become too small. The corresponding first-order coefficient becomes large and a treatment based on perturbation theory is no longer valid. This problem can be surpassed by a level-shift technique.[46] It has been shown recently that a small value of the level shift (up to $0.4\,E_h$) does not significantly affect the estimate of the J constant.[47] We examined the effect of the level shift on the magnetic coupling constant for the anhydrous manganese paddlewheel. The results obtained within the FC approximation are shown in Table 4 and in Figure 5. The difference between the coupling constants calculated with level shifts of 0.1 and $0.2\,E_h$ is only $1.2\ cm^{-1}$, between 0.1 and $0.3\,E_h$ less than $2\ cm^{-1}$. This means that our results are almost not affected by the level-shift parameter. Finally, a CASPT2(10,10) calculation with a level-shift value of $0.1\,E_h$, but with all electrons correlated, yields $J=-20.0\ cm^{-1}$.

 © 2011 Wiley-VCH Verlag GmbH & Co. KGaA, Weinheim

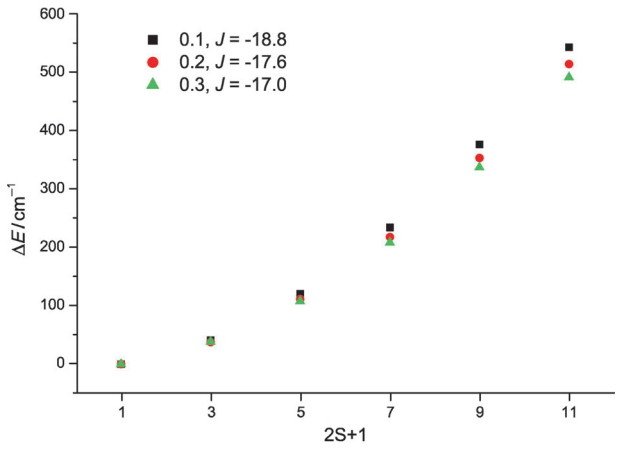

Figure 5. Impact of level shift on the state's energy differences for the anhydrous manganese paddlewheel.

The broken-symmetry approach was also used for this compound. While the high-spin state has ten unpaired electrons with parallel spins, the broken symmetry state is described by five spin-up electrons in one manganese and five spin-down electrons in the other. Equations (8) and (9) yield the same magnetic coupling constants. Lack of an experimental value for this complex makes us to compare these results with CASPT2. The hybrid B3LYP functional overestimates the magnetic exchange coupling constant ($J=-31.7\ cm^{-1}$) compared to the CASPT2 value. Like in the cases of the dicopper acetate compounds, the double-hybrid functional is superior to B3LYP.

By using the unprojected expression of Ruiz et al. [Eq. (12)]:[48]

$$J^{BS} = -\frac{E_{HS} - E_{BS}}{4S_1S_2 + 2S_2} \qquad (12)$$

J values from both functionals are closer to the CASPT2 result (Table 4). However, Equation (12) has been mainly proposed for strong coupled systems and its applicability is still a subject of debate.

3.3. Dinuclear Cobalt(II) Paddlewheel

As for the manganese compound, literature data for the cobalt acetate compounds are rare. Only a few crystal structures have been reported for the hydrated cobalt paddlewheel, with varying metal-metal distances. Normally, it varies between 2.69 Å and 2.86 Å,[49–51] indicating an antiferromagnetic nature. There are also cases where the distance is much smaller (2.27 Å), forming a short bond with a $\sigma^2\pi^4\delta^2\delta^{*2}\pi^{*4}$ electronic configuration.[52] Experimental data for the anhydrous Co^{II} paddlewheel have not been reported. In all the compounds studied experimentally, the ligand sphere of the metal is saturated, either by a water molecule or by other ligands. Here, we study the structure of the dicobalt formate with open metal sites. The optimized UMP2 geometry for the HS state displays a Co-Co distance of 2.74 Å, which is within the range of the experimental values.

Earlier,[53] we have shown that spin–orbit coupling (SOC) is mandatory for a complete description of the electronic structure of Co compounds. This holds mainly for octahedral and square-pyramidal complexes of cobalt.[54] In the paddlewheel geometry, each cobalt has a distorted square-pyramidal shape. The isolated Co^{2+} ion has a d^7 electronic configuration that comprises 120 microstates if each spin and angular momentum component is counted separately. The ^4F ground state splits into a $^4T_{1g}$ ground state and into excited $^4T_{2g}$ and $^4A_{2g}$ states in an octahedral ligand field. In a tetrahedal ligand field, the order of the states is reversed. In order to understand the magnetic properties of the anhydrous dicobalt acetate, we studied the electronic configuration of each metal center separately. Each cobalt atom is coordinated by four formate oxygen atoms, but it also interacts weakly with the other metal atom, experiencing in that way a distorted square-pyramidal ligand field. By removing the unpaired electrons of the other metal ion (keeping the geometry fixed) we can obtain the energy levels of the d orbitals of the first metal ion. This can be achieved by substituting the neighboring cobalt by a closed-shell ion such as Mg^{2+}, keeping the correct charge of the molecule. The Mg^{2+} ion was represented by a large effective core potential.[55] For simplicity, we shall denote this model as "CoMg" model. A second model was also used, in which one of the two Co^{2+} ions was replaced by a point charge ("PC" model).

The configuration of the d orbitals of Co^{2+} in an octahedral field is $t_{2g}^5e_g^2$. Due to a Jahn–Teller distortion, the ligand field reduces to D_{4h} symmetry. Our first target was to obtain molecular orbitals which provide a balanced description of the different electronic states of the d^7 Co^{2+} system in the ligand field of the paddlewheel structure. Therefore, a SA-CASSCF(7,5) calculation was performed, averaged over the lowest seven quartet states, with the five d orbitals as active space. This calculation predicted that the d_z^2 orbital is the most stable. d_{xz} and d_{yz} are only 4.3 mE_h higher in energy and d_{xy} as much as 20.8 mE_h. The $d_{x^2-y^2}$ orbital is destabilized by the antibonding interaction with the ligand oxygen atoms and more than 50 mE_h higher in energy. The left and right side of Figure 6 show the orbital energies of each isolated Co^{2+} ion in the field created by the ligand sphere of the paddlewheel structure. Both CoMg and PC models yielded the same sequence and almost the same energy differences between the d-orbital levels.

Table 5 shows the energy differences between the first five quartet states as obtained from SA-CASSCF(7,5) calculations for both models. SA-CASSCF(7,5) calculations on the CoMg model revealed that the 28-fold degenerate ^4F ground state of Co^{2+} splits into five new states. The ground state is 1^4E, with the first and second excited states 1^4B_2 and 2^4B_2 being only 307 and 392 cm^{-1} higher in energy, respectively (Figure 7a, left and right side). The next two states, 2^4E and $^4A_1$, are much higher in energy, at 8228 and 12635 cm^{-1}, respectively. For the PC model the values of the energy gaps between the ground state and the 2^4B_2, 2^4E and $^4A_1$ states are almost similar, while for the first excited state the predicted difference is about half of that of the CoMg model.

Table 5 also contains the SOC results for the splitting of the five quartet states that originate from the ^4F state of the isolat-

 © 2011 Wiley-VCH Verlag GmbH & Co. KGaA, Weinheim

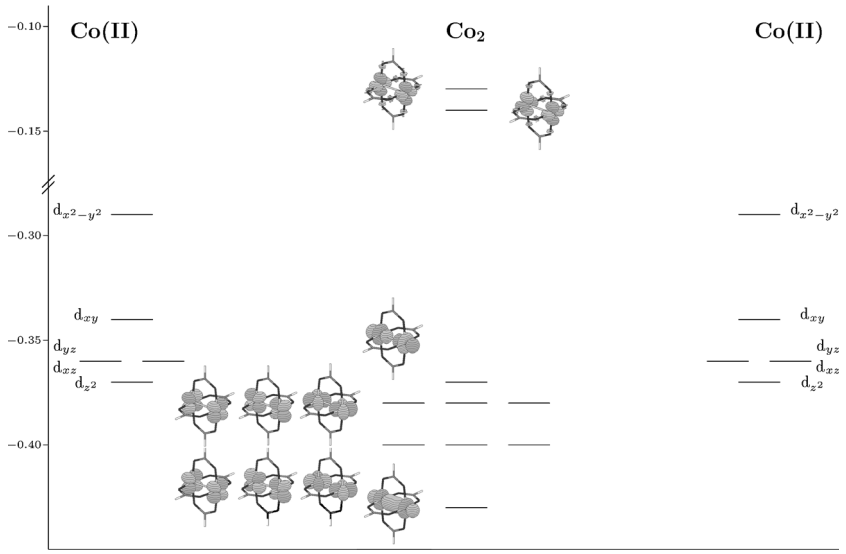

Figure 6. 3d orbitals of one Co^{II} atom in the ligand field of the paddlewheel structure (left, right), and the ten 3d-type orbitals of the anhydrous dicobalt formate (center) used in the (14,10) active space (energies in E_h).

Table 5. Ligand-field- and spin-orbit splittings of the ^4F ground state of Co^{2+} in the environment of the paddlewheel structure. Energies are in cm^{-1}.

		CoMg Model	PC Model 0[a,b]	16[a]	40[a]	120[a]
$1^4E(8)$[b]	$E_{1/2}(2)$[c]	0	0	0	0	0
	$E_{1/2}(2)$			42	41	41
	$E_{1/2}(2)$			446	427	431
	$E_{1/2}(2)$			617	605	619
$1^4B_2(4)$	$E_{1/2}(2)$	307	175	1079	1071	1086
	$E_{1/2}(2)$			1201	1170	1159
$2^4B_2(4)$	$E_{1/2}(2)$	392	432	1629	1619	1588
	$E_{1/2}(2)$			1643	1620	1611
$2^4E(8)$	$E_{1/2}(2)$	8228	8007		8178	8140
	$E_{1/2}(2)$				8500	8449
	$E_{1/2}(2)$				8840	8801
	$E_{1/2}(2)$				9208	9206
$^4A_1(4)$	$E_{1/2}(2)$	12635	12616		13346	10464
	$E_{1/2}(2)$				13353	11502

[a] N_{SOC}, dimension of the SOC-CI. [b] Without SOC. The degeneracy of the states is given in parentheses. [c] With SOC.

ed Co^{2+} ion. In the CoMg model, a spin-orbit configuration-interaction (SOCI) calculation of the full d^7 system can easily be done. This is not the case for the dinuclear Co compound. Therefore, we analyzed the influence of the spin-orbit coupling on the energy differences of the lowest electronic states for the PC model. First, we diagonalized the SOC Hamiltonian in the full space of 120 states belonging to the d^7 configuration ($N_{SOC}=120$). As can be seen in the last column of Table 5, no degeneracies remain except from the two-fold Kramers degeneracy of a system with an odd number of electrons. The 1^4E ground state splits into four components that belong to the irreducible representation $E_{1/2}$. The two $^4B_2$ states also split into two $E_{1/2}$ states. Then, we limited the SOCI matrix to the 40 states that span the ^4F and ^4P manifold ($N_{SOC}=40$). Even in a 16-state SOCI calculation, the relative energies of the first four Kramers doublets remained constant. Thus, we conclude that it is sufficient to include those states of the dinuclear compound that arise from the coupling of the lowest three quartet states (^4E and two $^4B_2$) of each Co^{2+} ion.

Figure 7a shows the relative energies of the uncoupled 1^4E, 1^4B_2 and 2^4B_2 states and the resulting four lowest spin-orbit coupled $E_{1/2}$ states, which are dominated by the $E_{1/2}$ state. SOC stabilizes the $E_{1/2}$ ground state by about 700 cm^{-1} and increases the energy difference between the ground state and the two $^4B_2$ states. For the PC model without SOC, the gap between the two first states is 175 cm^{-1} (Table 5). The gap increases to about 1100 cm^{-1} by SOC. The same behavior is observed for the second $^4B_2$ state, with SOC increasing the energy difference by about a factor of four. This considerable gap ($\approx$1 eV) between the first four states and the next two allows us to focus on the eight lower $E_{1/2}$ states. By coupling the two cobalts in the specific geometry, the doubly degenerate 1^4E and the two $^4B_2$ states will give rise to 16 septet states by exchange interaction. The energy gap between the first group of 16 septet states and the next 16 septet states is about 6570 cm^{-1}. This was calculated at the SA-CASSCF(14,10) level by averaging over the first 32 septet states. Figure 6 (center) shows the ten magnetic orbitals used in the SA-CASSCF(14,10) calculation and their relative energies. These are formed from the 3d orbitals of the two Co^{2+} ions. As expected, the lowest orbital is the bonding $d_{z^2}+d_{z^2}$ molecular orbital. The bonding and antibonding combinations of the d_{xy}, d_{xz} and d_{yz} orbitals, as well as the antibonding $d_{z^2}-d_{z^2}$ orbital, are found 31 mE_h higher in energy. A significant energy gap (232 mE_h) separates the two $d_{x^2-y^2}\pm d_{x^2-y^2}$ molecular orbitals from the rest.

Starting with the orbitals from the SA-CASSCF(14,10) calculations averaging the 16 lowest septets, SA-CASSCF(14,10) calculations were performed to determine the energies of the low-lying quintet, triplet and singlet states in addition to those of the septets. In each calculation, the 16 states with same spin multiplicity were averaged. Table 6 shows the 64 low-lying states and their energy differences relative to the lowest $^7B_{1u}$ state. Since all of these states are derived from the same 1^4B_2, 2^4B_2 and 1^4E states of the two isolated metals in the ligand field of the paddlewheel structure, which are very close in energy, the SA-CASSCF orbitals determined for the high-multiplicity states yield a reasonable description also for the states with lower spins.

SA-CASSCF(14,10) theory predicts a septet ground state (1^7B_{1u}), with the first excited state (1^7B_{1g}) only 47 cm^{-1} higher in

 © 2011 Wiley-VCH Verlag GmbH & Co. KGaA, Weinheim

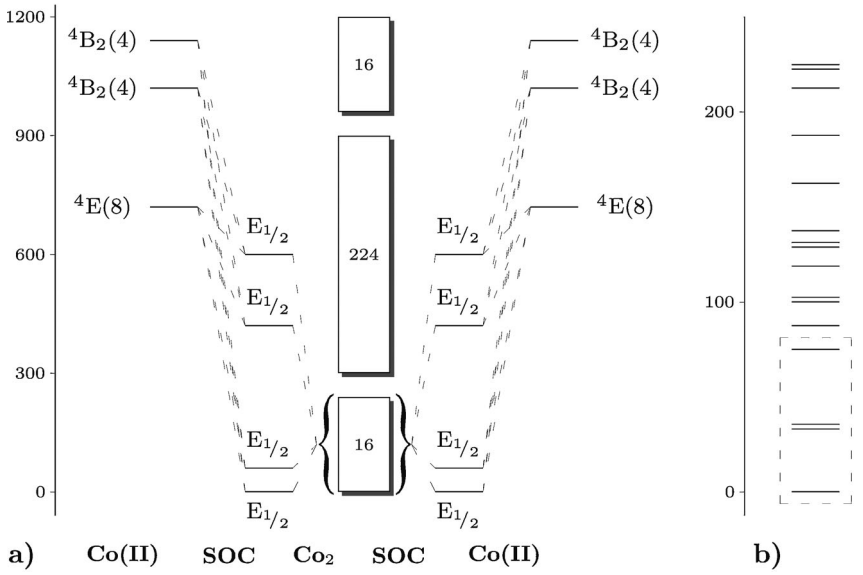

Figure 7. a) Splitting of the lowest states of one Co^{II} atom in the ligand field of the paddlewheel structure (left, right) by spin–orbit coupling (SOC) and exchange interaction. The energies of the 256 states of the anhydrous dicobalt formate (center) are not to scale; b) Energy levels of the 16 lowest states of the dinuclear compound.

Table 6. The 64 lowest states of anhydrous dicobalt acetate and their relative energy differences [cm^{-1}] as obtained from SA-CASSCF(14,10) calculations.

State	Energy	State	Energy	State	Energy	State	Energy
1^7B_{1u}	0	1^7B_{3u}	169	1^7B_{2g}	339	2^3B_{3g}	790
1^7B_{1g}	47	1^1B_{2g}	171	1^7B_{2g}	339	2^3B_{2g}	790
1^1A_g	118	1^1B_{3g}	171	3^5A_g	370	2^3B_{2u}	791
1^5A_g	137	1^3B_{2u}	184	3^7B_{1u}	558	2^3B_{3u}	791
1^1B_{1g}	139	1^3B_{3u}	184	2^7B_{2u}	634	2^5B_{2u}	810
1^5A_u	144	1^3B_{2g}	188	1^7B_{3u}	634	2^5B_{3u}	810
1^1B_{2u}	144	1^3B_{3g}	188	1^7A_g	666	2^1B_{2g}	811
1^1B_{3u}	144	1^5B_{2g}	209	4^7B_{1u}	692	2^1B_{3g}	811
2^1A_g	145	1^5B_{3g}	209	2^5B_{2g}	753	1^3A_g	822
1^3B_{1g}	158	3^3B_{1u}	210	2^5B_{3g}	753	4^3A_{1u}	822
1^3B_{1u}	158	2^5A_g	224	2^1B_{2u}	779	1^1B_{1u}	841
3^1A_g	163	1^5B_{1u}	226	2^1B_{3u}	779	4^1A_g	845
2^3B_{1u}	164	2^7B_{1u}	245	1^5B_{1u}	784	5^1A_g	1395
1^1A_u	164	1^7A_u	248	1^5B_{1g}	786	5^3A_{1u}	1405
1^3A_u	168	1^5B_{2u}	274	2^7B_{3g}	789	5^7B_{1u}	1417
1^7B_{2u}	169	1^5B_{3u}	274	2^7B_{2g}	789	5^5A_g	1426

energy. This means that the multi-reference analysis up to this point predicts a ferromagnetic compound. The lowest singlet state is 118 cm^{-1} higher than the ground state and the next 30 states are found within a range of 160 cm^{-1}. This complexity of states is a result of both space and spin degrees of freedom.

As in the mononuclear complexes, the whole pattern of low-lying states is completely changed as soon as SOC is included. For the complete molecule we coupled 16 septet, 16 quintet, 16 triplet and 16 singlet microstates. The coupling of all of the 64 states of Table 6 gives rise to 256 closely spaced states (Figure 7a, center). Each of these states is a linear combination of microstates with different spin multiplicities. Hence, we cannot longer refer to pure singlet, triplet, quintet or septet states. However, the ground state of the SOCI calculation has a major contribution of 22% from the 1^1A_1 microstate with minor contributions from microstates with other multiplicities. The first excited state is doubly degenerate, 33 cm^{-1} above the ground state, equally balanced between microstates of all four different spin multiplicities. The next two states are dominated by septet microstates (71% and 92%) and are located 75 and 87 cm^{-1} higher in energy, respectively. Eleven more states are about 220 cm^{-1} above the ground state. Figure 7b shows the relative energies of these 16 lowest states. The next 224 states are in a region between 500 and 3100 cm^{-1}, with small energy differences between them. The remaining 16 states are found between 3450 and 3600 cm^{-1}.

From the above we can conclude that the dinuclear cobalt compound and its electronic states cannot be described by a HDV Hamiltonian. A pronounced spin ladder between distinct spin states cannot be reproduced and information about the value of the magnetic coupling constant cannot be extracted. The dominant effect of the spin–orbit coupling on the SA-CASSCF wavefunction indicates that CASPT2 without SOC will provide no solution. An alternative would be to shift the CASSCF energies in the SOCI by CASPT2 correlation energies.[56] However, single-state CASPT2 calculations were tried on top of SS-CASSCF or SA-CASSCF wavefunctions, also with the level-shift technique, but they failed to reach convergence for the singlet, triplet and quintet states, due to their complexity.

Based on the SOCI calculations, the compound should behave like an antiferromagnet. At very low temperatures the magnetic susceptibility should be close to zero and then increase when the degenerate state at 33 cm^{-1} starts to be occupied at higher temperatures.

3.4. Trinuclear Chromium(III) Formate

Oxo-centered trigonal carboxylate-bridged $[M_3O(OOCR)_6L_3]^{n+}$ is a family of inorganic compounds that have attracted considerable attention due to the competing exchange interactions in such systems (Figure 1b). Before analyzing the magnetic behavior of these complexes and presenting our results, a short discussion about the structures is in place.

Compounds of this family show many different structures, depending on the oxidation state and the ligand sphere of the metals. In the simplest case, all three metals are in oxidation state III and the complex displays D_{3h} symmetry. For the chro-

 © 2011 Wiley-VCH Verlag GmbH & Co. KGaA, Weinheim

mium acetate, the Cr–μ_3-O distance is in the range of 1.88 to 1.94 Å and the Cr–Cr distance is between 3.28 and 3.36 Å.[57–61] The differences are a result of the different axial ligands. For example, the replacement of water by a stronger donor like pyridine in the axial site leads to a lenghtening of the trans Cr–μ_3-O bonds.[58]

3.4.1. Anhydrous Trinuclear Chromium(III) Formate

A UMP2/def2-TZVP optimization gave a Cr–μ_3-O distance of 1.85 Å and a Cr–Cr distance of 3.21 Å. For technical reasons, all of the multi-reference calculations were performed in C_{2v} symmetry. While the core of the compound is spatially symmetric, the spin symmetry of the triangle is not perfect and this gives rise to interesting magnetic properties for this family of compounds. Cr^{III} has a d^3 electronic configuration and thus a (9,9) active space is a reasonable starting point. Figure 8 shows the orbitals included in the (9,9) active space. It is composed of combinations of the t_{2g} orbitals of each chromium. The MOs composed of the e_g combinations were significantly higher in energy and were excluded from our study.

Competing exchange interactions increase the complexity of the trimetallic compounds. The main reason for the complexity is the existence of spin frustration of the triangle formed by the three metals. Spin frustration is defined as the inability of spins to adopt their preferred alignments, which are obtained through exchange coupling with neighboring spins. For example, the singlet state of such a compound with a trivanadium(III) core has a metal with spin $S_z=1$, another with $S_z=-1$ and one with $S_z=0$. This "classical" picture of spins does not correspond to an equilateral triangle. In the case of the trichromium compound, the spins should be $S_z=\pm 3/2$ on each of the three centers. Such spin populations, however, are unstable with respect to a weak perturbation transforming the equilateral triangle to an isosceles one. Such a distortion might arise from the Jahn–Teller instability of the ^2E state in C_3 symmetry or from a packing effect.[62] In the case of $[Cr_3O(OOCH)_6]^+$, the magnetic Jahn–Teller effect is negligible and its ground state is a degenerate ^2E state.

The HDV model spin Hamiltonian was first applied to the $[M_3O(OOCR)_6L_3]^{n+}$ complexes by Kambe,[63] who introduced an exchange coupled trimer model where isotropic exchange interactions between ions are antiferromagnetic and assumed to be equal. The eigenvalues of the HDV Hamiltonian are shown on the left side of Figure 9. Later studies on trichromium complexes showed that at low temperatures (1.6 K), dynamic distortions lead to an isosceles trimer, which is described by a model with two exchange coupling constants, J_0 and J_0+J_1, with $|J_1J_0^{-1}| \ll 1$ for the legs and the base, respectively.[64] J_0 varies between -12 to $-10\ cm^{-1}$, depending again on the coordination sphere of the metal.[9] This is the driving force of the exchange coupling, showing a purely antiferromagnetic nature. Since the ratio $|J_1J_0^{-1}|$ is much smaller than one, results from EPR spectroscopy and INS can be fitted to equilateral as well as isosceles models.[61]

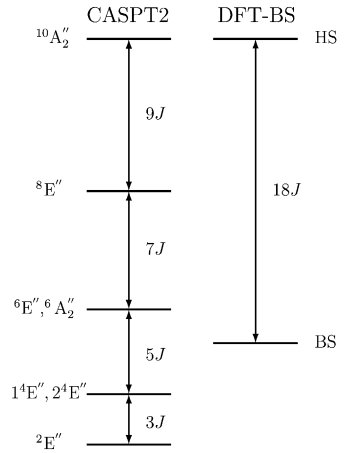

Figure 9. Energy differences of the spin states from CASPT2 and DFT-BS calculations on trichromium formate.

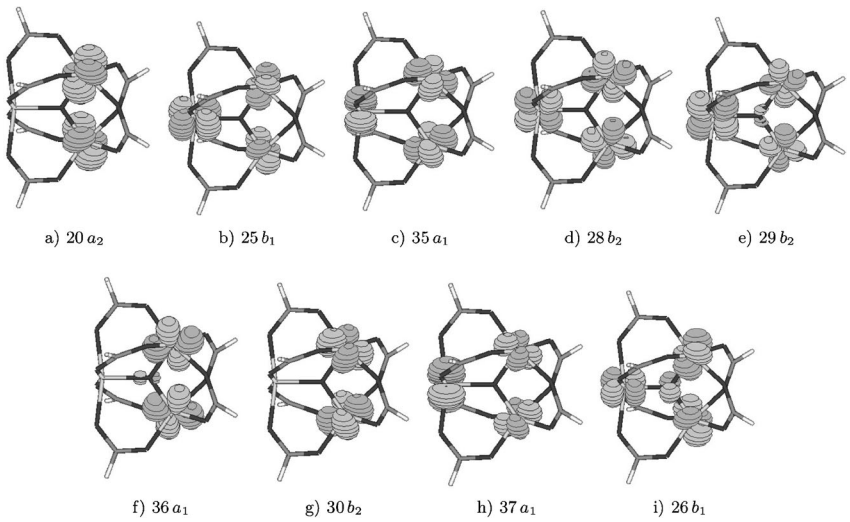

Figure 8. Magnetic orbitals of the (9,9) active space of the anhydrous trichromium formate.

The splittings of the spin states from the exchange couplings can be summarized as follows: The main exchange parameter J_0 creates five distinguishable states of different total spin $S_T=S_1+S_2+S_3$, …, 1/2, forming a fully discernible spin ladder. The coupling constant J_0 can be easily calculated from energy differences using Equation (3). By adding the effect of the second coupling constant $J_1\neq 0$, the degeneracies appearing from the equilateral model are removed. The ground state then splits into two doublets, the quartet into four new states, the sextet into three, and the octet into two

 © 2011 Wiley-VCH Verlag GmbH & Co. KGaA, Weinheim

states. In our multi-reference treatment, we calculated all possible spin states of the trinuclear compound. The first step was the calculation of the electronic states for the various spin multiplicities with the complete-active-space configuration-interaction method (CASCI). Even if CASSCF is more reliable and accurate, CASCI is a good starting point for large systems in view of its reduced computational cost with respect to CASSCF.

CASCI and SA-CASSCF calculations averaged over all states of Figure 9 were performed. In addition, single-state CASSCF calculations using the SA-CASSCF orbitals as starting orbitals were also performed. Table 7 shows the results from all of these methods. CASCI(9,9) and CASSCF(9,9) calculations failed to predict the antiferromagnetic nature of the trichromium molecules. All calculations predicted a weak ferromagnetic coupling.

Table 7. J values for the anhydrous trichromium formate [cm^{-1}].

Method	J	
	(9,9)	(6,6)[a]
CASCI	2.9	–
SA-CASSCF	0.6	0.6
CASSCF	2.1	0.5
CASPT2	−15.8	−16.2

[a] Pair approximation. See the text for details.

By adding contributions from dynamical correlation, the description of the system changes significantly. CASPT2(9,9) predicts correctly the antiferromagnetic nature of the trichromium formate. A spin ladder between the degenerate doublets, quartets, sextets, octets and decet was calculated (Figure 9), with a magnetic exchange constant $J=-15.8\ cm^{-1}$ being comparable with its experimental counterparts for the trichromium acetate hydrate, which are in the region from −12 to $-10\ cm^{-1}$. This means that the inclusion of effects due to dynamical correlation is mandatory for a complete description of the magnetic phenomena of this family of compounds. The ground state comprises the two doublets $^2A_2$ and $^2B_1$ in the computationally applied C_{2v} symmetry, which correspond to a $^2E''$ state in the underlying D_{3h} symmetry.

We also estimated the magnetic coupling constant by a *pair approximation*.[16] The coupling constant between a pair of metal centers is calculated while the third center is substituted by a point charge or a cation. This treatment is similar to the substitution of one cobalt with a Mg^{2+} ion in the dicobalt paddlewheel. In the trichromium case, a +3 charge is needed and thus, an Al^{3+} ion was used. The active space was restricted to (6,6), corresponding to the d electrons of the two remaining metals. Results for the pair approximation are shown in Table 7. These are comparable with the full compound for the SA-CASSCF ($J=0.6\ cm^{-1}$) and single-state CASSCF ($J=0.5\ cm^{-1}$) wavefunctions. The inclusion of dynamical correlation again leads to an antiferromagnetic coupling. CASPT2(6,6) calculations based on SA-CASSCF(6,6) wavefunctions yielded $J=-16.2\ cm^{-1}$, which is almost identical with the CASPT2(9,9) result ($J=-15.8\ cm^{-1}$).

The broken-symmetry approach was also tested for the trichromium systems, applying Equation (9). The difference of the expectation values of the S^2 operator for the high-spin and broken-symmetry states is 18, in agreement with other approaches.[16,65] Due to the high symmetry, $J_{12}=J_{13}=J_{23}=J$. The spin-density isosurface of the broken-symmetry state is presented in Figure 10. The spin density is identical for every

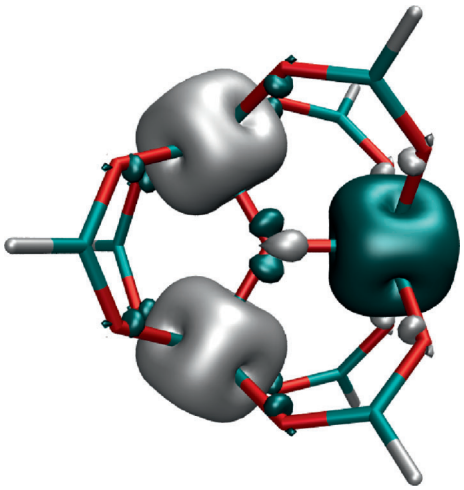

Figure 10. Spin-density iso surfaces (±0.01) of the broken-symmetry state (B2-PLYP) of the trichromium formate.

center and is composed of the three singly occupied d orbitals on each metal atom. Minor contributions are also observed from the formate oxygens and, mainly, from the central oxygen. Thus, the metal centers are coupled mainly through the central oxygen. The B3LYP and B2-PLYP functionals were used, with B3LYP giving a result ($J=-11.7\ cm^{-1}$) closer to the CASPT2 coupling constant.

3.4.2. Hydrated Trinuclear Chromium(III) Formate

Results similar to those for the anhydrous system were obtained for the hydrated chromium formate. The structure of the latter was obtained by adding one H_2O molecule to every open metal site and optimizing only the coordinates of the water molecules, keeping the rest frozen, focusing our attention on the effect of the H_2O ligands.

CASSCF(9,9) theory erroneously predicts a ferromagnetic behavior. The value of $J=0.96\ cm^{-1}$ is similar to the one obtained for the anhydrous compound. SA-CASSCF(9,9) calculations yielded a similar estimate ($0.7\ cm^{-1}$). As in the anhydrous case, the addition of dynamical correlation alters the results, now predicting an antiferromagnetic coupling. Based on the SA-CASSCF(9,9) wavefunction, single-state CASPT2(9,9) calculations reproduced the spin-ladder of Figure 9. The result of $J=-11.5\ cm^{-1}$ is within the range of the experimental data for the trichromium acetate hydrate (−12 to $-10\ cm^{-1}$).

The pair approximation was also tested on the hydrated complex. In this case, all of the methods, that is, SA-CASSCF ($0.65\ cm^{-1}$), single-state CASSCF ($0.68\ cm^{-1}$) and CASPT2

 © 2011 Wiley-VCH Verlag GmbH & Co. KGaA, Weinheim

($-11.5\ cm^{-1}$) gave almost the same results as obtained for the complete compound. Finally, the broken-symmetry approach succeeded to correctly predict the antiferromagnetic coupling. Again, the B3LYP result was closer to CASPT2 than B2-PLYP.

4. Conclusions

The main objective of the present study was to compare various quantum chemical methods (both wavefunction- and density-functional based) for the calculation of magnetic properties of di- and trinuclear transition-metal complexes. The *J* values of all of the systems studied in the present work are summarized in Table 8.

Table 8. Overview of *J* results for the anhydrous metal formates [cm^{-1}].

	Cu_2	Mn_2	Cr_3
CASSCF	−16.8	−6.70	0.6[a]
CASPT2[b]	−91.3	−20.0	−15.8[a]
B3LYP	−467	−31.7	−11.7
B2-PLYP[c]	−260	−22.4	−3.0

[a] Results from the (9,9) active space. [b] All orbitals correlated. [c] All orbitals correlated for the PT2 part.

It has been known for a long time that accounting for effects of dynamical correlation is important for an accurate prediction of the magnetic exchange coupling constant.[11] This was confirmed by our CASSCF and CASPT2 calculations, in agreement with previous DDCI results.[8,38] In our work, the basis-set dependence turned out not to be that pronounced. Trustworthy results could be obtained using the cc-pVTZ basis set for the metal ions and the cc-pVDZ basis set for all of the other atoms. While a treatment of dynamical correlation effects at the CASPT2 level is essential, the corresponding CASPT2 calculations on the dimanganese paddlewheel were hampered by the intruder-state problem, which was solved by applying a level-shift technique.

At the DFT level, the BS approach with common GGA and hybrid functionals significantly overestimated the magnetic coupling constant of the copper paddlewheel. Recent BS studies with the M06 family of functionals and range-separated hybrid functionals have reached good agreement with the experimental values.[41,42] Herein, we calculated this coupling constant with similar accuracy with the double-hybrid B2-PLYP functional. For the weak interaction between the two metal centers of the manganese paddlewheel, BS results were consistent with the CASPT2 results, with the B2-PLYP value being slightly closer. With respect to the dinuclear complexes, we conclude that the B2-PLYP functional yields more reliable results than those obtained at the B3LYP level.

The inclusion of spin–orbit coupling was mandatory for the proper theoretical description of the dicobalt formate compound. The complexity of the 64 uncoupled states was revealed from SOCI calculations, which gave rise to 256 closely spaced states. Due to the complexity of the uncoupled states, CASPT2 calculations for the low-spin states failed to reach convergence.

For the trichromium system, we found small energy differences between the spin states. The state-averaged CASSCF method seemed to describe the states better than what is possible by means of single-state CASSCF or CASCI calculations. Again, accounting for effects of dynamical correlation is important for the trichromium system as well. Without accounting for dynamical correlation effects, the antiferromagnetic nature of the trichromium molecule could not be reproduced. The CASPT2(9,9) results, however, were in good agreement with the available experimental data. We furthermore note that the pair approximation yielded very reasonable results. At the DFT level, the BS approach succeeded to correctly describe the magnetic coupling constant of the trichromium system, but in this case B3LYP outperformed B2-PLYP.

Acknowledgement

The authors thank Prof. V. Staemmler for helpful discussions and unpublished data from calculations on the copper paddlewheel. K.D.V. and W.K. thank the Deutsche Forschungsgemeinschaft (DFG) for support through the Center for Functional Nanostructures (grant No. C3.3). A.M. acknowledges a fellowship from the Alexander von Humboldt Foundation. K.F. thanks the DFG for support through the Collaborative Research Center CRC/Transregio 88 "3MET" (grant No. A1).

Keywords: broken-symmetry approach · computational chemistry · density functional calculations · magnetic exchange coupling · paddlewheel structures

[1] M. Dincă, J. R. Long, *Angew. Chem.* **2008**, *120*, 6870 – 6884; *Angew. Chem. Int. Ed.* **2008**, *47*, 6766 – 6779.
[2] S. S. Chui, S. M. Lo, J. P. Charmant, A. G. Orpen, I. D. Williams, *Science* **1999**, *283*, 1148 – 1150.
[3] J. Y. Lee, O. K. Farha, J. Roberts, K. A. Scheidt, S. B. T. Nguyen, J. T. Hupp, *Chem. Soc. Rev.* **2009**, *38*, 1450 – 1459.
[4] K. Schlichte, T. Kratzke, S. Kaskel, *Microporous Mesoporous Mater.* **2004**, *73*, 81 – 88.
[5] G. J. Kubas, *Chem. Rev.* **2007**, *107*, 4152 – 4205.
[6] M. N. Leuenberger, D. Loss, *Nature* **2001**, *410*, 789 – 793.
[7] A. Rodríguez-Fortea, P. Alemany, S. Alvarez, E. Ruiz, *Chem. Eur. J.* **2001**, *7*, 627 – 637.
[8] I. de P. R. Moreira, F. Illas, *Phys. Chem. Chem. Phys.* **2006**, *8*, 1645 – 1659.
[9] R. D. Cannon, R. White in *Progress in Inorganic Chemistry, Vol. 36* (Ed.: S. J. Lippard), Wiley, New York, **1988**, pp. 195 – 298.
[10] A. Henschel, K. Gedrich, R. Kraehnert, S. Kaskel, *Chem. Commun.* **2008**, 4192 – 4194.
[11] P. de Loth, P. Cassoux, J. P. Daudey, J. P. Malrieu, *J. Am. Chem. Soc.* **1981**, *103*, 4007 – 4016.
[12] K. Fink, R. Fink, V. Staemmler, *Inorg. Chem.* **1994**, *33*, 6219 – 6229.
[13] L. Noodleman, *J. Chem. Phys.* **1981**, *74*, 5737 – 5743.
[14] L. Noodleman, E. R. Davidson, *Chem. Phys.* **1986**, *109*, 131 – 143.
[15] K. Yamaguchi, H. Fukui, T. Fueno, *Chem. Lett.* **1986**, 625 – 628.
[16] H. Fliegl, K. Fink, W. Klopper, C. E. Anson, A. K. Powell, R. Clérac, *Phys. Chem. Chem. Phys.* **2009**, *11*, 3900 – 3909.
[17] A. Görling, M. Levy, *Phys. Rev. B* **1993**, *47*, 13105 – 13113.
[18] S. Grimme, *J. Chem. Phys.* **2006**, *124*, 034108.
[19] T. Schwabe, S. Grimme, *J. Phys. Chem. Lett.* **2010**, *1*, 1201 – 1204.
[20] F. Weigend, M. Häser, H. Patzelt, R. Ahlrichs, *Chem. Phys. Lett.* **1998**, *294*, 143 – 152.

 © 2011 Wiley-VCH Verlag GmbH & Co. KGaA, Weinheim

[21] C. Hättig, F. Weigend, *J. Chem. Phys.* **2000**, *113*, 5154 – 5161.
[22] R. Ahlrichs, M. Bär, M. Häser, H. Horn, C. Kölmel, *Chem. Phys. Lett.* **1989**, *162*, 165 – 169.
[23] Turbomole V6.3; a development of Universität Karlsruhe (TH) and Forschungszentrum Karlsruhe GmbH, 1989 – 2007, TURBOMOLE GmbH, since 2007. Available from http://www.turbomole.com, **2011**.
[24] B. N. Figgis, R. L. Martin, *J. Chem. Soc.* **1956**, 3837 – 3846.
[25] E. B. Shamuratov, A. S. Batsanov, K. T. Sharipov, Y. T. Struchkov, T. Azizov, *Koord. Khim.* **1994**, *20*, 754 – 755.
[26] C. Prestipino, L. Regli, J. G. Vitillo, F. Bonino, A. Damin, C. Lamberti, A. Zecchina, P. L. Solari, K. O. Kongshaug, S. Bordiga, *Chem. Mater.* **2006**, *18*, 1337 – 1346.
[27] MOLPRO, a package of ab initio programs written by H. J. Werner, P. J. Knowles, version 2006.1. R. D. Amos, A. Bernhardsson, A. Berning, P. Celani, D. L. Cooper, M. J. O. Deegan, A. J. Dobbyn, F. Eckert, C. Hampel, G. Hetzer, P. Knowles, T. Korona, R. Lindh, A. W. Lloyd, S. McNicholas, F. R. Manby, W. Meyer, M. E. Mura, A. Nicklass, P. Palmieri, R. Pitzer, G. Rauhut, M. Schütz, U. Schumann, H. Stoll, A. J. Stone, R. Tarroni, T. Thorsteinsson, H. Werner.
[28] K. L. Schuchardt, B. T. Didier, T. Elsethagen, L. Sun, V. Gurumoorthi, J. Chase, J. Li, T. L. Windus, *J. Chem. Inf. Model.* **2007**, *47*, 1045 – 1052.
[29] A. D. Becke, *Phys. Rev. A* **1988**, *38*, 3098 – 3100.
[30] J. P. Perdew, K. Burke, M. Ernzerhof, *Phys. Rev. Lett.* **1996**, *77*, 3865 – 3868.
[31] J. Tao, J. P. Perdew, V. N. Staroverov, G. E. Scuseria, *Phys. Rev. Lett.* **2003**, *91*, 146401 – 146404.
[32] V. N. Staroverov, G. E. Scuseria, J. Tao, J. P. Perdew, *J. Chem. Phys.* **2003**, *119*, 12129 – 12137.
[33] A. D. Becke, *J. Chem. Phys.* **1993**, *98*, 5648 – 5652.
[34] C. T. Lee, W. T. Yang, R. G. Parr, *Phys. Rev. B* **1988**, *37*, 785 – 789.
[35] F. Weigend, R. Ahlrichs, *Phys. Chem. Chem. Phys.* **2005**, *7*, 3297 – 3305.
[36] H. U. Güdel, A. Stebler, A. Furrer, *Inorg. Chem.* **1979**, *18*, 1021 – 1023.
[37] F. Aquilante, T. B. Pedersen, R. Lindh, B. O. Roos, A. S. de Merás, H. Koch, *J. Chem. Phys.* **2008**, *129*, 024113.
[38] R. Maurice, K. Sivalingam, D. Ganyushin, N. Guihéry, C. de Graaf, F. Neese, *Inorg. Chem.* **2011**, *50*, 6229 – 6236.
[39] J. Miralles, J.-P. Daudey, R. Caballol, *Chem. Phys. Lett.* **1992**, *198*, 555 – 562.
[40] J. Miralles, O. Castell, R. Caballol, J.-P. Malrieu, *Chem. Phys.* **1993**, *172*, 33 – 43.
[41] P. Rivero, I. de P. R. Moreira, F. Illas, G. E. Scuseria, *J. Chem. Phys.* **2008**, *129*, 184110.
[42] R. Valero, R. Costa, I. de P. R. Moreira, D. G. Truhlar, F. Illas, *J. Chem. Phys.* **2008**, *128*, 114103.
[43] O. A. Vydrov, G. E. Scuseria, *J. Chem. Phys.* **2006**, *125*, 234109.
[44] Z. Fu, J. Yi, Y. Chen, S. Liao, N. Guo, J. Dai, G. Yang, Y. Lian, X. Wu, *Eur. J. Inorg. Chem.* **2008**, 628 – 634.
[45] D. A. Pantazis, V. Krewald, M. Orio, F. Neese, *Dalton Trans.* **2010**, *39*, 4959 – 4967.
[46] N. Forsberg, P.-A. Malmqvist, *Chem. Phys. Lett.* **1997**, *274*, 196 – 204.
[47] N. Queralt, D. Taratiel, C. de Graaf, R. Caballol, R. Cimiraglia, C. Angeli, *J. Comput. Chem.* **2008**, *29*, 994 – 1003.
[48] E. Ruiz, J. Cano, S. Alvarez, P. Alemany, *J. Comput. Chem.* **1999**, *20*, 1391 – 1400.
[49] J. Catterick, M. B. Hursthouse, P. Thornton, A. J. Welch, *J. Chem. Soc. Dalton Trans.* **1977**, 223 – 226.
[50] J. E. Davies, A. V. Rivera, G. M. Sheldrick, *Acta Crystallogr. Sect. B* **1977**, *33*, 156 – 158.
[51] N. Benbellat, K. S. Gavrilenko, Y. L. Gal, O. Cador, S. Gohlen, A. Gouasmia, J.-M. Fabre, L. Ouahab, *Inorg. Chem.* **2006**, *45*, 10440 – 10442.
[52] F. A. Cotton, R. Poli, *Inorg. Chem.* **1987**, *26*, 3652 – 3653.
[53] K. Fink, C. Wang, V. Staemmler, *Inorg. Chem.* **1999**, *38*, 3847 – 3856.
[54] M. Kurmoo, *Chem. Soc. Rev.* **2009**, *38*, 1353 – 1379.
[55] A. Nicklass, M. Dolg, H. Stoll, H. Preuss, *J. Chem. Phys.* **1995**, *102*, 8942 – 8953.
[56] C. de Graaf, C. Sousa, *Int. J. Quantum Chem.* **2006**, *106*, 2470 – 2478.
[57] S. C. Chang, G. A. Jeffrey, *Acta Crystallogr. Sect. B* **1970**, *26*, 673 – 683.
[58] F. A. Cotton, W. Wang, *Inorg. Chem.* **1982**, *21*, 2675 – 2678.
[59] T. Glowiak, H. Kozlowski, L. S. Erre, G. Micera, *Inorg. Chim. Acta* **1996**, *248*, 99 – 102.
[60] R. D. Cannon, U. A. Jayasooriya, F. E. Sowrey, C. Tilford, A. Little, J. P. Bourke, R. D. Rogers, J. B. Vincent, G. J. Kearley, *Inorg. Chem.* **1998**, *37*, 5675 – 5677.
[61] V. Psycharis, C. P. Raptopoulou, A. K. Boudalis, Y. Sanakis, M. Fardis, G. Diamantopoulos, G. Papavassiliou, *Eur. J. Inorg. Chem.* **2006**, 3710 – 3723.
[62] O. Kahn, *Chem. Phys. Lett.* **1997**, *265*, 109 – 114.
[63] K. Kambe, *J. Phys. Soc. Jpn.* **1950**, *5*, 48 – 51.
[64] M. Honda, M. Morita, M. Date, *J. Phys. Soc. Jpn.* **1992**, *61*, 3773 – 3785.
[65] H. Wei, B. Wang, Z. Chen, *Chem. Phys. Lett.* **2005**, *407*, 147 – 152.

Received: July 19, 2011
Revised: October 10, 2011
Published online on November 7, 2011

 © 2011 Wiley-VCH Verlag GmbH & Co. KGaA, Weinheim